

See discussions, stats, and author profiles for this publication at: <https://www.researchgate.net/publication/259252355>

A novel tamoxifen derivative, ridaifen-F, is a nonpeptidic small-molecule proteasome inhibitor

ARTICLE *in* EUROPEAN JOURNAL OF MEDICINAL CHEMISTRY · NOVEMBER 2013

Impact Factor: 3.45 · DOI: 10.1016/j.ejmech.2013.11.009 · Source: PubMed

CITATIONS

3

READS

67

13 AUTHORS, INCLUDING:



[Tatsuki Kunoh](#)

Okayama University

22 PUBLICATIONS 144 CITATIONS

SEE PROFILE



[Masafumi Shionyu](#)

Nagahama Institute of Bio-Science and Tec...

20 PUBLICATIONS 361 CITATIONS

SEE PROFILE



Original article

A novel tamoxifen derivative, ridaifen-F, is a nonpeptidic small-molecule proteasome inhibitor



Makoto Hasegawa^{a,*}, Yukari Yasuda^a, Makoto Tanaka^a, Kenya Nakata^b, Eri Umeda^b, Yanwen Wang^b, Chihiro Watanabe^b, Shoko Uetake^b, Tatsuki Kunoh^a, Masafumi Shionyu^a, Ryuzo Sasaki^a, Isamu Shiina^{b,**}, Tamio Mizukami^a

^a Faculty of Bioscience, Nagahama Institute of Bio-Science and Technology, 1266 Tamura-cho, Nagahama, Shiga 526-0829, Japan

^b Department of Applied Chemistry, Faculty of Science, Tokyo University of Science, 1-3 Kagurazaka, Shinjuku-ku, Tokyo 162-8601, Japan

ARTICLE INFO

Article history:

Received 19 August 2013

Received in revised form

2 November 2013

Accepted 6 November 2013

Available online 16 November 2013

Keywords:

Proteasome inhibitors

Tamoxifen derivatives

Structure–activity relationship (SAR)

Docking studies

ABSTRACT

In a survey of nonpeptide noncovalent inhibitors of the human 20S proteasome, we found that a novel tamoxifen derivative, RID-F (compound **6**), inhibits all three protease activities of the proteasome at submicromolar levels. Structure–activity relationship studies revealed that a RID-F analog (RID-F-S*4, compound **25**) is the smallest derivative compound capable of inhibiting proteasome activity, with a potency similar to that of RID-F. Kinetic analyses of the inhibition mode and competition experiments involving biotin-belactosin A (a proteasome inhibitor) binding indicated that the RID-F derivatives interact with the protease subunits in a different manner. Culturing of human cells with these compounds resulted in accumulation of ubiquitinated proteins and induction of apoptosis. Thus, the RID-F derivatives may be useful lead chemicals for the generation of a new class of proteasome inhibitors.

© 2013 Elsevier Masson SAS. All rights reserved.

1. Introduction

Eukaryotic cells have two different pathways for protein degradation: the lysosomal pathway and the ubiquitin–proteasome pathway. The lysosomal pathway breaks down endogenous and endocytosed exogenous proteins in a relatively nonspecific manner to provide amino acids as building materials for protein synthesis. In contrast, the ubiquitin–proteasome system is the major machinery for regulated proteolysis of endogenous proteins. Protein degradation by the ubiquitin–proteasome system is initiated by the labeling of targeted proteins with polyubiquitin chains in an intra- or extracellular signal-dependent manner [1]. Degradation of ubiquitinated proteins by the 26S proteasome plays a pivotal role in the regulation of a number of cellular processes, such as cell cycle progression, cell growth, proliferation, differentiation, apoptosis, gene transcription, and signal transduction [2]. Aberrant degradation of key regulatory proteins by the proteasome perturbs these processes, causing uncontrolled cell cycle progression and a decrease in cell death, both of which are hallmarks of tumorigenesis [3].

Several proteasome inhibitors have been proposed as anticancer drugs [1,4–8]. One of these inhibitors, the peptide boronate bortezomib, has been approved for the clinical treatment of multiple myeloma and mantle cell lymphoma [2]. The toxic boronate pharmacophore, however, causes severe side effects [9]. More recently, the tetrapeptide epoxyketone carfilzomib, which is an epoxomicin analog, has also been approved for the treatment of multiple myeloma [10–12]. In addition to being targeted in the treatment of various blood-borne tumors, proteasome inhibition has been suggested for the treatment of solid tumors [4], parasites, inflammation, immune diseases, and muscular dystrophies [13], encouraging development of new types of proteasome inhibitors with enhanced efficacy and fewer side effects [5].

The 26S proteasome is a large protein complex of ~2.5 MDa that consists of two subcomplexes with different functions: the 19S regulatory complex and the 20S catalytic core. The 20S catalytic core is a barrel-shaped protein composed of seven α subunits (α 1–7) and seven β subunits (β 1–7). The 19S regulatory complex also consists of multiple subunits and caps the 20S barrel at one or both ends. The 19S regulatory cap recognizes, unfolds, and translocates polyubiquitinated substrates into the 20S catalytic core, where the substrates are degraded. In the 20S proteasome core, the β 1, β 2, and β 5 subunits act as proteases, with caspase-(peptidyl)glutamyl peptide hydrolase, PGPH), trypsin-, and chymotrypsin-like activities,

* Corresponding author. Tel.: +81 749 64 8114.

** Corresponding author. Tel.: +81 3 3260 4271.

E-mail addresses: m_hasegawa@nagahama-i-bio.ac.jp (M. Hasegawa), shiina@rs.kagu.tus.ac.jp (I. Shiina).

respectively [1,2]. All of these hydrolytic activities are manifested through a threonine residue at the active site (Thr1).

Most of the dominant proteasome inhibitors, including bortezomib and carfilzomib, are short peptides that mimic substrates. The pharmacophores bound to the C-terminus of the peptide framework bind covalently to Thr1 in the 20S catalytic core active site. However, peptide bonds are easily degraded by endogenous proteases, and the reactive pharmacophores are susceptible to nucleophilic attack and are thus short-lived *in vivo*. Therefore, nonpeptide and noncovalent synthetic proteasome inhibitors would be valuable. More recently, a number of investigations have focused on inhibitors that are peptidic but noncovalent as part of efforts to overcome the drawbacks associated with covalent inhibitors [14]. These compounds include ritonavir [15], amino-benzylstatine [16], 3,4,5-trimethoxy-L-phenylalanine derivatives [17], 5-methoxy-1-indanone dipeptide benzamides [18], lipopeptides [19], N- and C-capped dipeptides derived from S-homophenylalanine [20,21], and TMC-95A [22,23] and its linear mimetic derivatives [24,25]. However, only a few inhibitors with both noncovalent and nonpeptidic characteristics have been reported [26].

Tamoxifen (TAM) binds to the estrogen receptor (ER) in place of the endogenous growth hormone, 17 β -estradiol, suppressing proliferation of ER-positive breast cancer cells and inducing apoptosis [27]. However, it has been reported that TAM provokes apoptosis through an ER-independent pathway [28,29]. Indeed, TAM induces apoptosis of ER-negative cells through perturbation of the mitochondrial membrane potential [30]. Ridaifen-B (RID-B,

see also Table 1), a TAM derivative, has been shown to induce apoptosis through the same pathway but with higher potency than TAM [30].

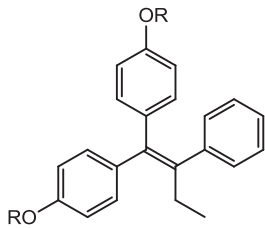
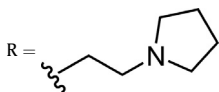
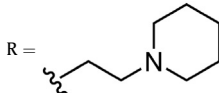
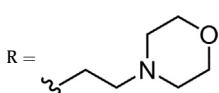
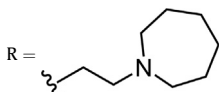
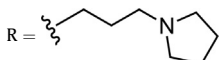
To find new noncovalent and nonpeptidic proteasome inhibitors, in this study we surveyed proteasome inhibition using a series of TAM derivatives. We found that RID-A, -B, -D, and -F inhibit the function of the 20S proteasome catalytic core *in vitro*. As RID-F was the most potent inhibitor of the three different enzymatic activities of the proteasome, we examined the structure–activity relationships of RID-F analogs with the hope of generating proteasome inhibitors that can be used to treat a wider range of diseases with minimal side effects.

2. Results and discussion

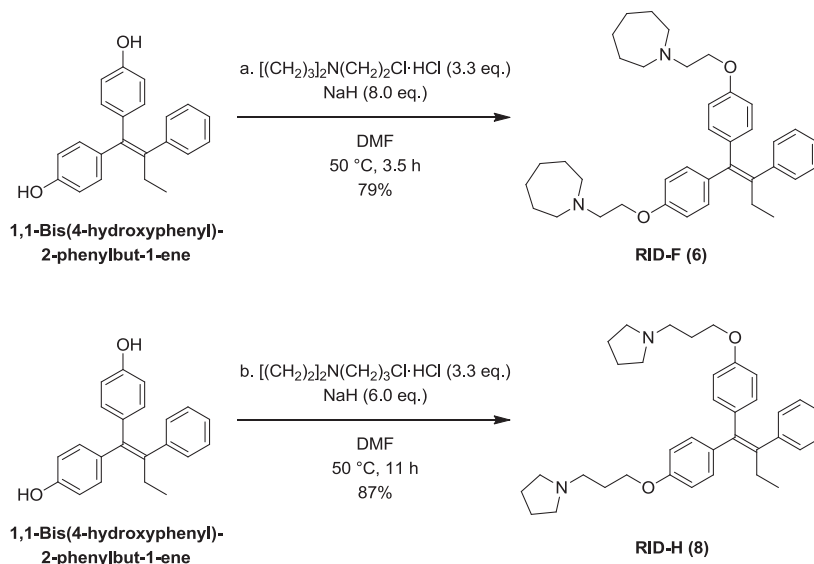
2.1. Synthesis of RID-F, RID-H, and other RID-F derivatives (RID-F-S*X)

Synthesis of RIDs A–H (compounds 1–8) was conducted according to methods described in our previous reports and patents [31–35]. The synthetic pathways for producing new compounds 6 and 8–29 are depicted in Schemes 1–11. As an example, Scheme 1 illustrates the transformation of the phenol moieties of 1,1-bis(4-hydroxyphenyl)-2-phenylbut-1-ene into the corresponding aminoethyl ethers of RID-F (compound 6) and RID-H (compound 8) in dimethylformamide (DMF). 1,1-Bis(4-hydroxyphenyl)-2-phenylbut-1-ene was easily synthesized using a three-component coupling reaction involving

Table 1
Inhibition of human 20S proteasome activity by ridaifens (RIDs).

Compound number			IC ₅₀ (μM) ^a		
			CT-L	T-L	PGPH
1	RID-A	R = CH ₂ CH ₂ N(CH ₃) ₂	3.36 ± 0.86	>10	2.99 ± 0.41
2	RID-B	R = 	6.56 ± 0.14	>10	6.37 ± 0.28
3	RID-C	R = 	>10	>10	7.50 ± 0.18
4	RID-D	R = 	7.19 ± 0.28	>10	7.26 ± 0.27
5	RID-E	R = CH ₂ CH ₂ N(C ₂ H ₅) ₂	>10	>10	>10
6	RID-F	R = 	0.64 ± 0.14	0.34 ± 0.12	0.43 ± 0.08
7	RID-G	R = CH ₂ CH ₂ CH ₂ N(CH ₃) ₂	>10	NT	NT
8	RID-H	R = 	>10	NT	NT

^a IC₅₀ values denote concentrations of the compounds required for 50% inhibition of the activities (see “Experimental section”). Values are means of three experiments. CT-L, chymotrypsin-like activity; T-L, trypsin-like activity; PGPH, peptidylglutamyl peptide hydrolase activity. NT, not tested.



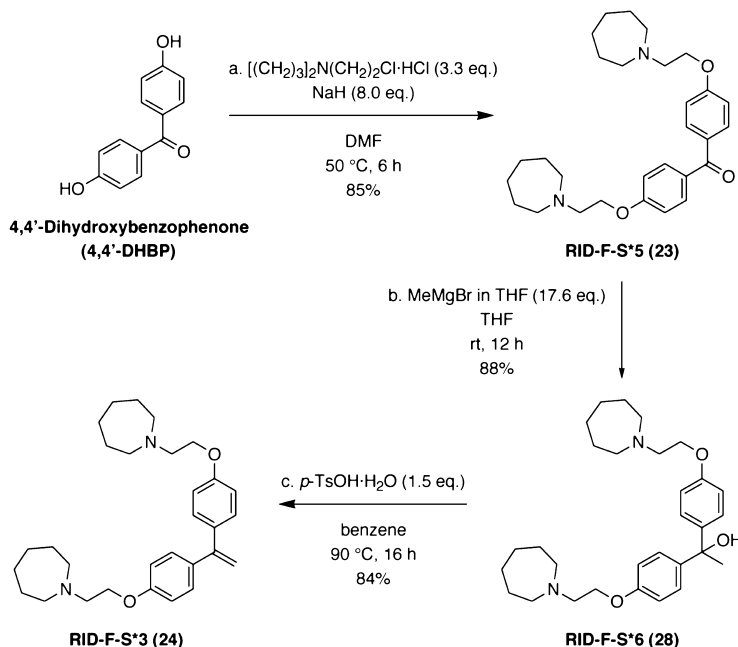
Reagents and conditions: (a) $[(CH_2)_3]_2N(CH_2)_2Cl \cdot HCl$ (3.3 eq.), NaH (8.0 eq.), DMF, 50 °C, 3.5 h, 79%; (b) $[(CH_2)_2]_2N(CH_2)_3Cl \cdot HCl$ (3.3 eq.), NaH (6.0 eq.), DMF, 50 °C, 11 h, 87%.

Scheme 1. Synthesis of RID-F (6) and RID-H (8) from 1,1-bis(4-hydroxyphenyl)-2-phenylbut-1-ene.

aromatic aldehyde, cinnamyltrimethylsilane, and anisole in the presence of $HfCl_4$ [31–33].

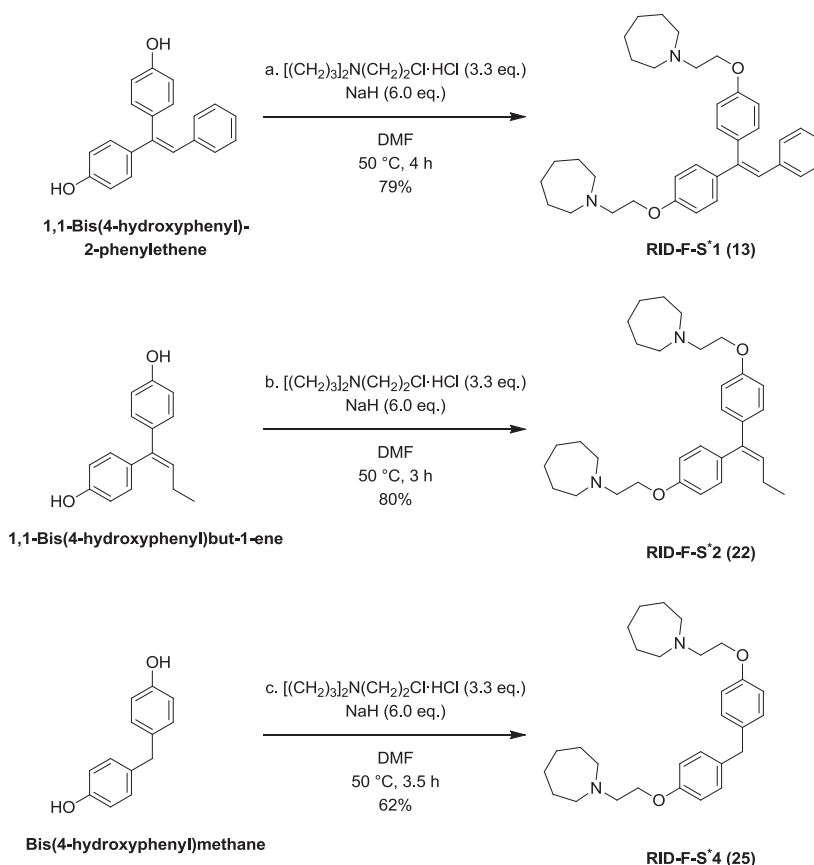
RID-F-S*3 (compound **24**), 1,1-bis[4-[2-(azepan-1-yl)ethoxy]phenyl]ethene, was synthesized from 4,4'-dihydroxybenzophenone (4,4'-DHBP) via a chemical approach involving *O*-alkylation, C1 segment installation, and acid-mediated dehydration, as shown in Scheme 2. First, the phenol moieties of 4,4'-DHBP were converted

into the corresponding aminoethyl ethers with 85% yield by *O*-alkylation with *N*-(2-chloroethyl)hexahydro-1*H*-azepine HCl, and successive alkylation of the carbonyl group in RID-F-S*5 (compound **23**) using methyl Grignard reagent was carried out in tetrahydrofuran (THF) to produce the 1,1-diphenylethanol derivative RID-F-S*6 (compound **28**), with 88% yield. Finally, treatment of tertiary alcohol **28** with *p*-TsOH was attempted in benzene, and the facile



Reagents and conditions: (a) $[(CH_2)_3]_2N(CH_2)_2Cl \cdot HCl$ (3.3 eq.), NaH (8.0 eq.), DMF, 50 °C, 6 h, 85%; (b) MeMgBr in THF (1.12 M, 17.6 eq.), THF, room temperature, 12 h, 88%; (c) *p*-TsOH·H₂O (1.5 eq.), benzene, 90 °C, 16 h, 84%.

Scheme 2. Synthesis of RID-F-S*5 (23), RID-F-S*6 (28), and RID-F-S*3 (24) from 4,4'-dihydroxybenzophenone (4,4'-DHBP).



Reagents and conditions: (a) $[(CH_2)_3]_2N(CH_2)_2Cl \cdot HCl$ (3.3 eq.), NaH (6.0 eq.), DMF, 50 °C, 4 h, 79%; (b) $[(CH_2)_3]_2N(CH_2)_2Cl \cdot HCl$ (3.3 eq.), NaH (6.0 eq.), DMF, 50 °C, 3 h, 80%; (c) $[(CH_2)_3]_2N(CH_2)_2Cl \cdot HCl$ (3.3 eq.), NaH (6.0 eq.), DMF, 50 °C, 3.5 h, 62%.

Scheme 3. Synthesis of RID-F-S*1 (13), RID-F-S*2 (22), and RID-F-S*4 (25) from 1,1-bis(4-hydroxyphenyl)-2-phenylethene, 1,1-bis(4-hydroxyphenyl)but-1-ene, and bis(4-hydroxyphenyl)methane.

dehydration process resulted in successful synthesis of the desired molecule **24**, with 84% yield.

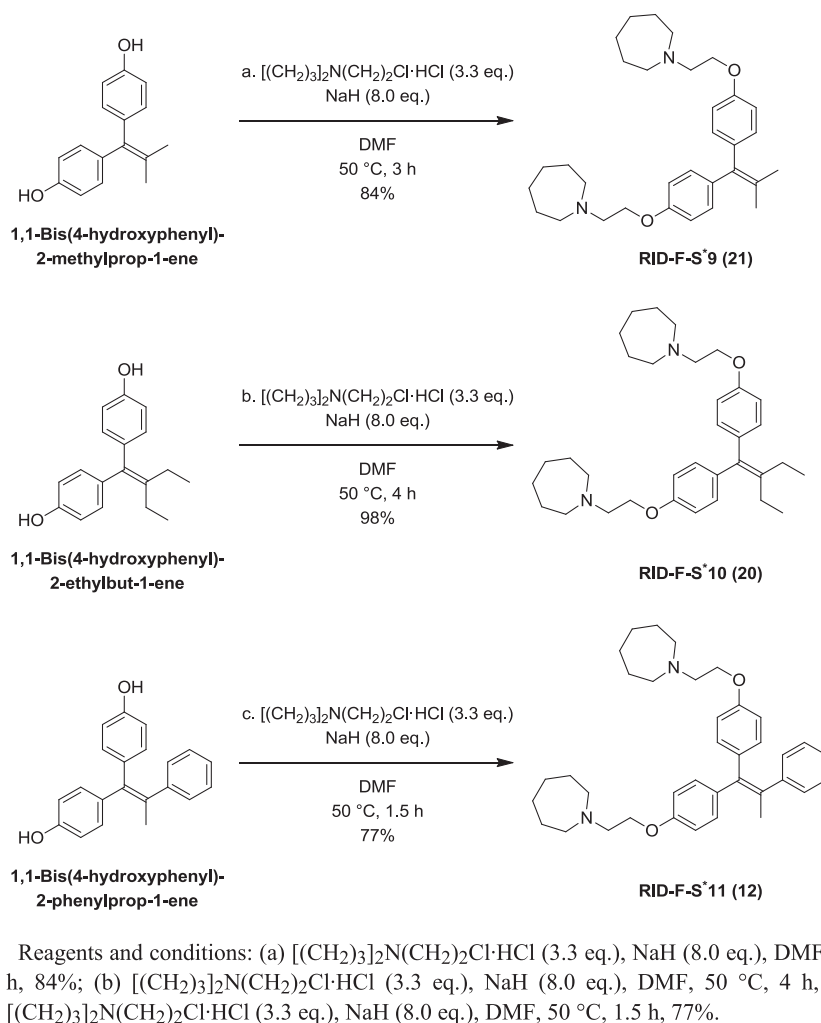
RID-F-S*13 (compound **9**), 1,1-bis{4-[2-(azepan-1-yl)ethoxy]phenyl}-2-cyclohexyl-2-phenylethene, was synthesized using the Mukaiyama reductive coupling reaction [36,37] depicted in Scheme 3. First, cyclohexyl phenyl ketone was treated with an excess of 4,4'-DHBP in the presence of the low-valent titanium species generated from titanium(IV) chloride with zinc powder in THF to afford 1,1-bis(4-hydroxyphenyl)-2-cyclohexyl-2-phenylethene, the desired olefin, with 65% yield. Next, the phenol moieties of the cross-coupling product were transformed into the corresponding aminoethyl ethers by *O*-alkylation in DMF, with 83% yield. Thus, an efficient method for the preparation of compound **9** was established through two steps from commercially available 4,4'-DHBP. RID-F-S*17 (compound **17**) and RID-F-S*24 (compound **16**) were also synthesized from 4,4'-DHBP with 6-undecanone or 7-tridecanone using the Mukaiyama reductive coupling reaction.

Other derivatives, RID-F-S*1 (compound **13**), RID-F-S*2 (compound **22**), RID-F-S*4 (compound **25**), RID-F-S*5 (compound **23**), RID-F-S*9 (compound **21**), RID-F-S*10 (compound **20**), RID-F-S*11 (compound **12**), RID-F-S*12 (compound **11**), RID-F-S*14 (compound **10**), RID-F-S*15 (compound **15**), RID-F-S*16 (compound **14**), RID-F-S*22 (compound **19**), RID-F-S*23 (compound **18**), RID-F-S*101 (compound **26**), RID-F-S*102 (compound **27**), and RID-F-S*103 (compound **29**) were synthesized from the corresponding commercially available bisphenols.

All RID physical properties (Mp, IR, 1H and ^{13}C NMR, and HR-MS) are shown in the Supporting information.

2.2. Inhibition of proteasome activities by ridafens

To identify new chemical moieties that function as proteasome inhibitors, we screened our in-house chemical libraries using an *in vitro* 20S proteasome inhibition assay. The potency of compounds was evaluated based on inhibition of the human 20S chymotrypsin-like (CT-L), trypsin-like (T-L), and PGPH activities of the 20S proteasome catalytic core. The IC_{50} , indicating the concentration required for 50% inhibition of the respective enzymatic activity (see Experimental section), was determined for each compound. The aldehyde proteasome inhibitor MG132 (Z-LLL-H) was used as a standard and had IC_{50} values of 0.011, 2.1, and 0.12 μM against CT-L, T-L, and PGPH activities, respectively. Of the 8 TAM derivatives tested (RID-A–RID-H; Table 1), RID-A, -B, and -D showed significant inhibition of CT-L and PGPH activities, but they did not significantly inhibit T-L activity. TAM did not inhibit any of the three enzymatic activities of the proteasome (Supplementary Table S1). RID-F, which has two homopiperidine moieties at the R positions, inhibited all three activities of the proteasome and was the most potent of the ridafen compounds examined. The ridafens did not inhibit calpain or cathepsin at concentrations of $>10 \mu M$ (data not shown), which indicated that the ridafens are highly specific inhibitors of the protease activities of the proteasome.



Scheme 4. Synthesis of RID-F-S*9 (**21**), RID-F-S*10 (**20**), and RID-F-S*11 (**12**) from 1,1-bis(4-hydroxyphenyl)-2-methylprop-1-ene, 1,1-bis(4-hydroxyphenyl)-2-ethylbut-1-ene, and 1,1-bis(4-hydroxyphenyl)-2-phenylprop-1-ene.

2.3. Inhibition of proteasome activities by RID-F derivatives

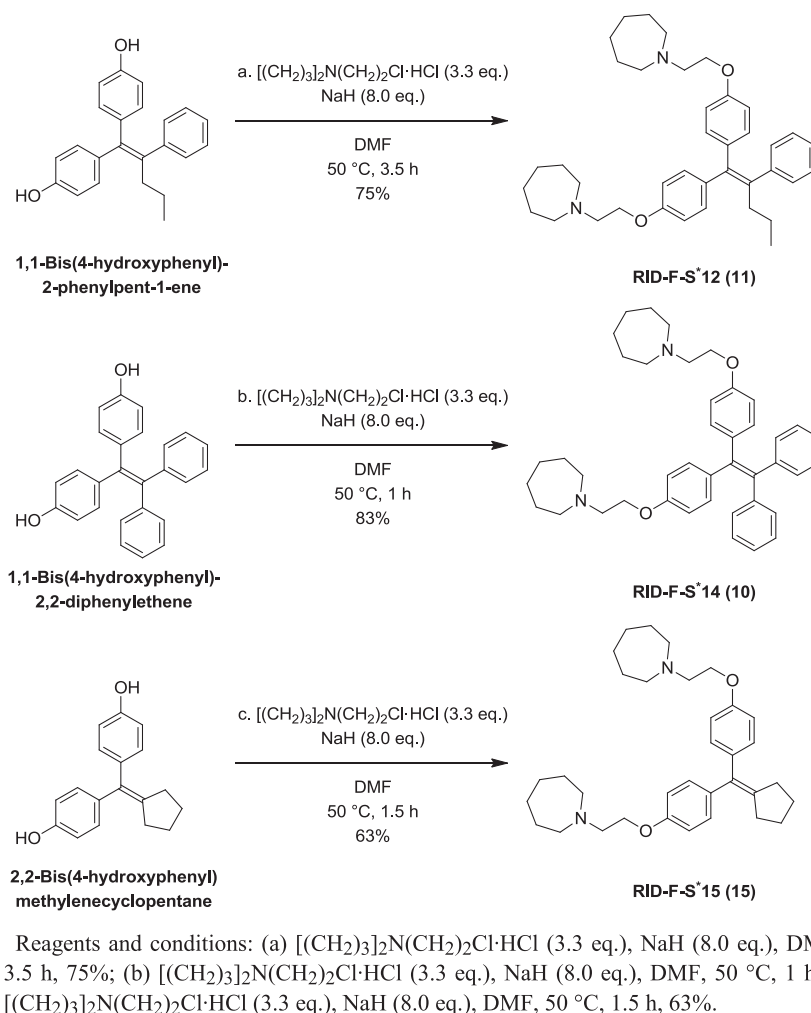
Because RID-F blocked proteasomal protease activities at concentrations in the submicromolar range, we examined the structure–activity relationships of various RID-F derivatives. RID-F has an sp^2 carbon atom at the center position (X in Table 2). The side structure at the X position was substituted with different aromatic ring(s). Table 2 summarizes the structures and inhibitory activities of these RID-F derivatives. A comparison of inhibition potency (IC_{50}) against CT-L activity indicated that RID-F (**6**), RID-F-S*11 (**12**), and RID-F-S*1 (**13**) were the most potent compounds. It should be noted that the volume of the vinyl benzene side structure and the inhibition potency against CT-L, T-L, and PGPH activities were similar for all three compounds.

To examine the contribution of side structures of the RID-F derivatives to the inhibition potency, we compared the volumes of the derivatives with the pocket volume of the proteasome active site. Side-structure models were built with energy minimization and molecular dynamics using Chem3D software (PerkinElmer Inc.). The solvent-excluded volumes of the side structures of RID-F (**6**), RID-F-S*11 (**12**), and RID-F-S*1 (**13**) calculated using Connolly's program [38] in Chem3D software were 119, 102, and 84 Å³, respectively. These values were close to the pocket volume (117 Å³) of the PGPH active site of the yeast 20S proteasome β 1 calculated

using Pocket-Finder, which is based on the LIGSITE algorithm [39]. Compounds with side structures smaller than (RID-F-S*16 (**14**) and RID-F-S*15 (**15**)) or larger than vinyl benzene (RID-F-S*13 (**9**) and RID-F-S*14 (**10**)) demonstrated low inhibition potency. These data suggest that vinyl benzene is an optimally sized side structure for inhibiting proteasomal protease activity.

Next, the side structure at the X position was substituted with aliphatic linear chains of varying lengths. Table 3 summarizes the structures and proteasome inhibitory activities of this series of compounds. RID-F-S*24 (**16**), RID-F-S*17 (**17**), and RID-F-S*23 (**18**) have long hydrocarbon chains; the volumes of their side structures were calculated to be 235, 201, and 167 Å³, respectively. These compounds demonstrated no inhibition of proteasome activity, indicating that hydrocarbon chains of more than eight carbon atoms in length interfere with the inhibitory activity of RID-F derivatives. RID-F-S*10 (**20**), RID-F-S*9 (**21**), RID-F-S*2 (**22**), RID-F-S*5 (**23**), and RID-F-S*3 (**24**), which have smaller and nonaromatic side structures, showed low inhibition potency.

To delineate the minimal structure necessary for proteasome inhibition, we examined a series of RID derivatives that had truncated side structures (Table 4). The smallest symmetric compound, RID-F-S*4 (**25**), demonstrated the highest inhibition potency, whereas, as seen with RID-F-S*110 (**30**) (Table 5) [40], removal of one of the two homopiperidine rings resulted in a critical loss of



Scheme 5. Synthesis of RID-F-S*12 (**11**), RID-F-S*14 (**10**), and RID-F-S*15 (**15**) from 1,1-bis(4-hydroxyphenyl)-2-phenylpent-1-ene, 1,1-bis(4-hydroxyphenyl)-2,2-diphenylethene, and 2,2-bis(4-hydroxyphenyl)methylenecyclopentane.

inhibition potency. Therefore, the structure of derivative RID-F-S*4 (**25**) appears to be the minimal structure possible for proteasome inhibition activity, and the presence of two homopiperidine rings appears to be crucial for inhibition.

2.4. Mode of RID-F derivative proteasome inhibition

Kinetic studies revealed that proteasome CT-L activity was inhibited by RID-F (**6**) in a noncompetitive manner, with a K_i of $0.58 \pm 0.14 \mu M$, whereas PGPH activity was inhibited in a competitive manner, with a K_i of $0.34 \pm 0.22 \mu M$ (Fig. 1). The other RID-F derivatives exhibited similar inhibition of proteasome CT-L and PGPH activities; RID-F-S*14 (**10**) and RID-F-S*1 (**13**) inhibited CT-L activity noncompetitively, with K_i values of $1.10 \pm 0.22 \mu M$ and $0.87 \pm 0.32 \mu M$, respectively, whereas they inhibited PGPH activity competitively, with K_i values of $1.02 \pm 0.15 \mu M$ and $0.67 \pm 0.29 \mu M$, respectively (data not shown). It has been shown that substrates of PGPH activity inhibit CT-L activity and that this inhibition is caused by binding of PGPH substrates to a noncatalytic CT-L site(s) rather than through binding to an active site [11]. Taken together, from these data we inferred that RID-F and its derivatives bind to both the active PGPH site and a noncatalytic CT-L site(s), resulting in inhibition of CT-L activity. As described below, the results of

docking simulations of ridaifens with the yeast counterpart of mammalian PGPH support this inference.

The chemical structures of the RID-F derivatives suggest that covalent binding to the proteasome is very unlikely. Indeed, labeling of proteasome subunits with a biotin-conjugated RID-F derivative failed to yield biotin-labeled proteins (data not shown). It has been shown that belactosin A preferentially inhibits both PGPH ($\beta 1$ subunit) and CT-L ($\beta 5$ subunit) by forming covalent linkages to the O^γ atom of the active site Thr1 [41]. Subunits covalently modified by biotin-labeled belactosin can be identified by Western blotting. Kinetic analyses showed that the RID-F derivatives inhibited PGPH activity in a competitive manner, suggesting direct interaction of the derivatives with the active site of the $\beta 1$ subunit (Fig. 1B).

We then examined whether RID-F derivatives could impede covalent modification by biotin-labeled belactosin. In agreement with previous results [41], we found that biotin-belactosin A primarily bound $\beta 1$ and $\beta 5$ but also bound $\beta 2$ with very low efficiency (Fig. 2). RID-F (**6**) and RID-F-S*4 (**25**) impeded binding of biotin-belactosin to $\beta 1$ (PGPH activity) in a dose-dependent manner (Fig. 2A and B). Both compounds inhibited CT-L activity in a noncompetitive manner (Fig. 1A), and therefore we expected that they do not reduce binding of belactosin to $\beta 5$ (CT-L activity). Contrary to this expectation, the compounds inhibited binding to

$\beta 5$, but the efficiency with which they inhibited binding to $\beta 5$ was much lower than that of $\beta 1$; at a concentration of 10 μM , the compounds almost completely inhibited binding of belactosin A to $\beta 1$, whereas binding to $\beta 5$ was still detectable at 100 μM . These results suggest that the region in which the RID-F compounds bind $\beta 5$ is proximal to the CT-L active site and partially overlaps the binding region of belactosin A. The concentration (10 μM) of the RID-F derivatives required to inhibit binding of belactosin to $\beta 1$ (PGPH activity) was much higher than the K_i (submicromolar levels) determined from kinetic analyses (Fig. 1A). There are several potential explanations for this difference: (i) the affinity of biotin-labeled belactosin A was higher than that of the substrate used for kinetic analyses, or (ii) the reversible inhibitor RID-F derivatives are eventually replaced by the covalent inhibitor, belactosin. MG132, which was used as a positive control for proteasomal protease inhibition, prevented biotin-belactosin A from forming covalent linkages to all subunits. RID-F-S*110 (**30**) showed little effect on belactosin binding (Fig. 2C), which was consistent with the result indicating that this compound has minimal inhibitory potency against proteasomal activity (Table 5). The possible mechanism by which RID-F derivatives prevent the binding of belactosin to the $\beta 2$ subunit (T-L activity) remains to be studied.

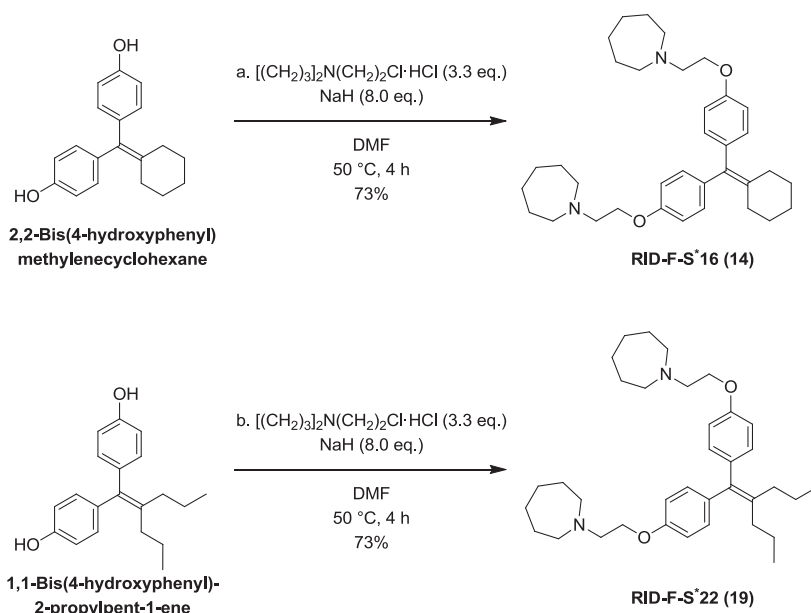
2.5. Cytotoxicity

We also evaluated the effect of the RID-F derivatives on proliferation of two human cell lines, human embryonic kidney 293 cells (HEK293, ER-negative) and HL-60 cells (ER-positive). Cells were treated with different concentrations of each compound for 48 h, after which the number of live cells was determined using a 3-(4,5-dimethylthiazol-2-yl)-2,5-diphenyltetrazolium bromide (MTT) assay. The CyT_{50} , defined as the concentration required for 50% inhibition of cell proliferation (see Experimental section), was determined for each compound, and the results are summarized in Tables 2–5. The compounds with poor inhibitory potency ($\text{IC}_{50} > 10 \mu\text{M}$) against CT-L activity *in vitro* were not cytotoxic, with

the exception of RID-F-S*22 (**19**), which significantly inhibited CT-L activity but was inexplicably noncytotoxic. Most of the cytotoxic compounds showed similar toxicity to both cell types, although some compounds (RID-F-S*12 (**11**), RID-F-S*11 (**12**) and RID-F-S*6 (**28**)) were more toxic to HL60 than HEK293 cells, and two compounds (RID-F-S*5 (**23**) and RID-F-S*103 (**29**)) were more toxic to HEK293 cells.

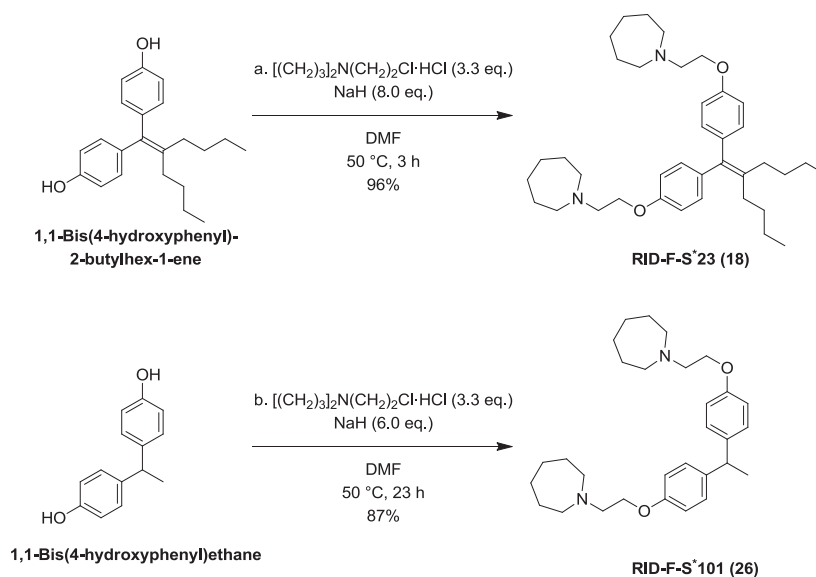
Is the cytotoxicity of RID-F derivatives attributable to their inhibition of proteasome activity? To address this question, we selected compounds that inhibited at least two of the three proteasome protease activities. The IC_{50} values of these compounds were plotted against the CyT_{50} values determined using HEK293 cells to estimate the correlation between proteasome inhibition and cytotoxicity (Fig. 3A). The correlation coefficients were 0.51 for CT-L activity and 0.48 for PGPH activity (Fig. 3B) but only 0.02 for T-L activity (Fig. 3C). Thus, it is very likely that the cytotoxicity of the RID-F derivatives is caused by their inhibition of proteasome CT-L and PGPH activities, whereas the inhibition of T-L activity is not associated with cytotoxicity. It is not known whether inhibition of either CT-L or PGPH activity alone is sufficient to cause cytotoxicity or if inhibition of both activities is required. Genetic studies have suggested that CT-L activity is essential for proteasome function, because mutational loss of CT-L activity causes a significant reduction in the degradation of proteasomal substrates [42,43]. Taken together, these data suggest that the inhibition of CT-L activity by RID-F derivatives may be linked to cell death. The CyT_{50} values of the RID-F derivatives were generally one order of magnitude higher than the corresponding IC_{50} values; restricted diffusion of the derivatives through the cell membrane may be responsible for this difference.

We next investigated the ability of the RID-F derivatives to inhibit proteasome function in cultured cells. HeLa cells were incubated with RID-F (**6**), RID-F-S*4 (**25**), or RID-F-S*110 (**30**), and the accumulation of ubiquitinated proteins was examined by Western blotting. A significant accumulation of multiple bands of high-molecular-weight ubiquitinated proteins was observed in



Reagents and conditions: (a) $[(\text{CH}_2)_3]_2\text{N}(\text{CH}_2)_2\text{Cl}\cdot\text{HCl}$ (3.3 eq.), NaH (8.0 eq.), DMF, 50 °C, 4 h, 73%; (b) $[(\text{CH}_2)_3]_2\text{N}(\text{CH}_2)_2\text{Cl}\cdot\text{HCl}$ (3.3 eq.), NaH (8.0 eq.), DMF, 50 °C, 4 h, 73%.

Scheme 6. Synthesis of RID-F-S*16 (**14**) and RID-F-S*22 (**19**) from 2,2-bis(4-hydroxyphenyl)methylenecyclohexane and 1,1-bis(4-hydroxyphenyl)-2-propylpent-1-ene.



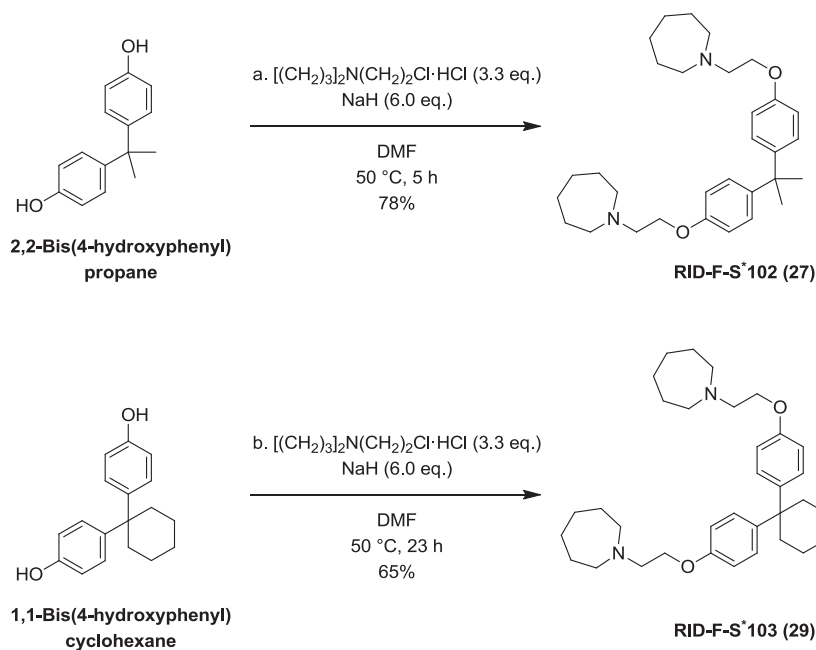
Reagents and conditions: (a) $[(\text{CH}_2)_3]_2\text{N}(\text{CH}_2)_2\text{Cl}\cdot\text{HCl}$ (3.3 eq.), NaH (8.0 eq.), DMF, 50 °C, 3 h, 96%; (b) $[(\text{CH}_2)_3]_2\text{N}(\text{CH}_2)_2\text{Cl}\cdot\text{HCl}$ (3.3 eq.), NaH (6.0 eq.), DMF, 50 °C, 23 h, 87%.

Scheme 7. Synthesis of RID-F-S*23 (18) and RID-F-S*101 (26) from 1,1-bis(4-hydroxyphenyl)-2-butylhex-1-ene and 1,1-bis(4-hydroxyphenyl)ethane.

cells treated with RID-F (6) and RID-F-S*4 (25) (Fig. 4, lanes 3 and 4). The accumulation of such proteins was minimal in cells treated with RID-F-S*110 (30), a compound that showed very low inhibition potency (Table 5). Accumulation of ubiquitinated proteins was also observed in lysates of cells treated with the known proteasome

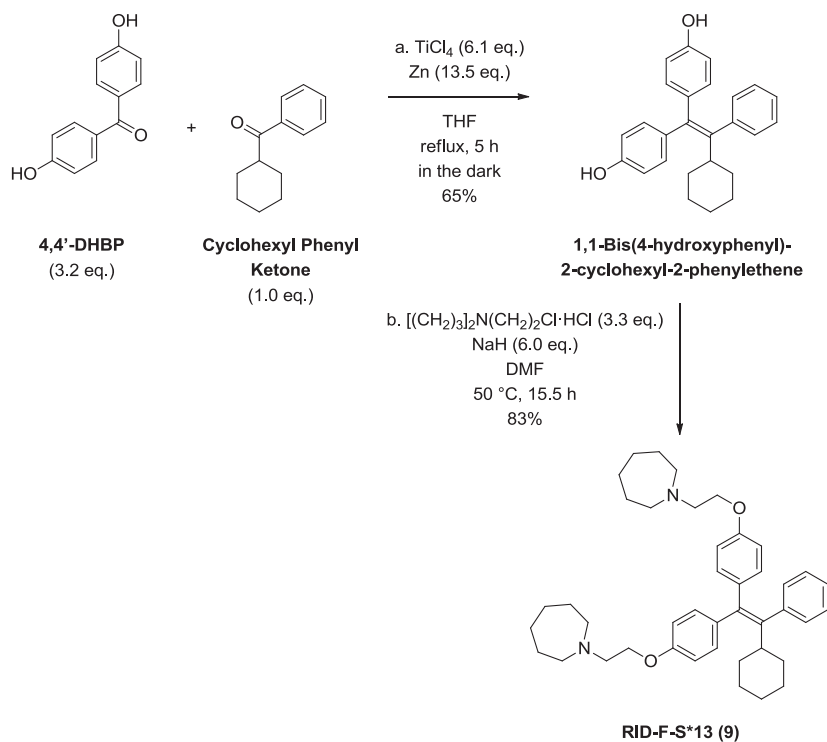
inhibitor, MG132 (Fig. 4, lane 2). These data indicate that RID-F derivatives inhibit proteasome activities in cells.

Abnormal accumulation of proteins resulting from the inhibition of proteasome activity has antiproliferative effects on cells, including induction of apoptosis. Therefore, we examined



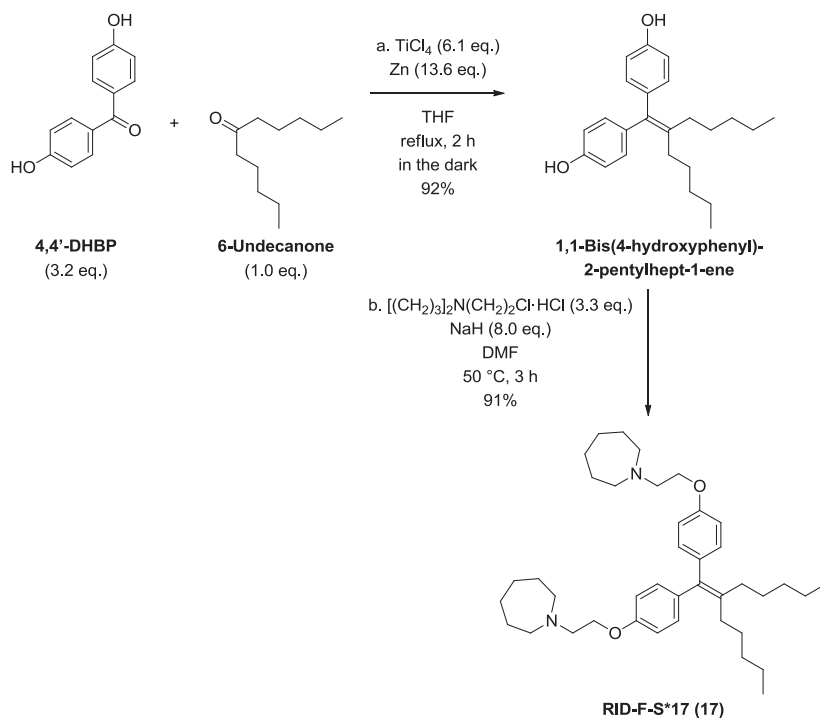
Reagents and conditions: (a) $[(\text{CH}_2)_3]_2\text{N}(\text{CH}_2)_2\text{Cl}\cdot\text{HCl}$ (3.3 eq.), NaH (6.0 eq.), DMF, 50 °C, 5 h, 78%; (b) $[(\text{CH}_2)_3]_2\text{N}(\text{CH}_2)_2\text{Cl}\cdot\text{HCl}$ (3.3 eq.), NaH (6.0 eq.), DMF, 50 °C, 23 h, 65%.

Scheme 8. Synthesis of RID-F-S*102 (27) and RID-F-S*103 (29) from 2,2-bis(4-hydroxyphenyl)propane and 1,1-bis(4-hydroxyphenyl)cyclohexane.



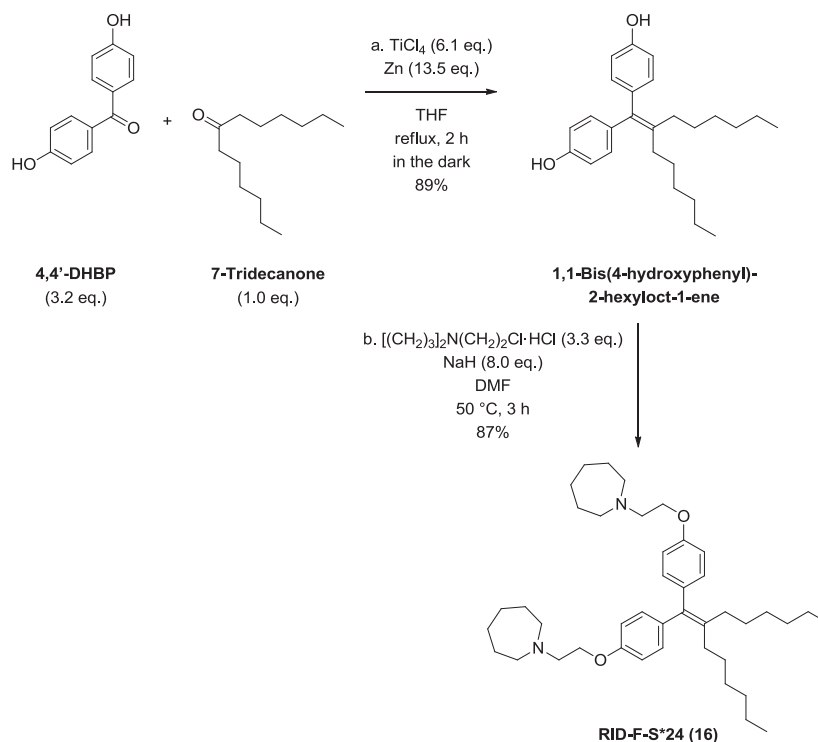
Reagents and conditions: (a) TiCl_4 (6.1 eq.), Zn (13.5 eq.), THF, reflux, 5 h in the dark, 65%; (b) $[(\text{CH}_2)_3]_2\text{N}(\text{CH}_2)_2\text{Cl}\cdot\text{HCl}$ (3.3 eq.), NaH (6.0 eq.), DMF, 50 °C, 15.5 h, 83%.

Scheme 9. Synthesis of RID-F-S*13 (9) from 4,4'-dihydroxybenzophenone (4,4'-DHBP) and cyclohexyl phenyl ketone.



Reagents and conditions: (a) TiCl_4 (6.1 eq.), Zn (13.6 eq.), THF, reflux, 2 h in the dark, 92%; (b) $[(\text{CH}_2)_3]_2\text{N}(\text{CH}_2)_2\text{Cl}\cdot\text{HCl}$ (3.3 eq.), NaH (8.0 eq.), DMF, 50 °C, 3 h, 91%.

Scheme 10. Synthesis of RID-F-S*17 (17) from 4,4'-dihydroxybenzophenone (4,4'-DHBP) and 6-undecanone.

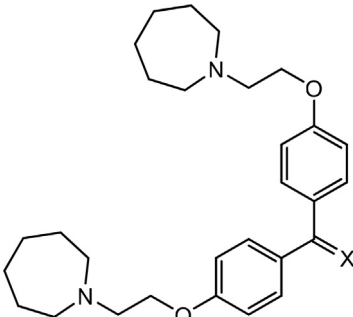
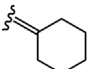
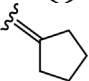


Reagents and conditions: (a) TiCl_4 (6.1 eq.), Zn (13.5 eq.), THF, reflux, 2 h in the dark, 89%;
(b) $[(\text{CH}_2)_3]_2\text{N}(\text{CH}_2)_2\text{Cl}\cdot\text{HCl}$ (3.3 eq.), NaH (8.0 eq.), DMF, 50 °C, 3 h, 87%.

Scheme 11. Synthesis of RID-F-S*24 (16) from 4,4'-dihydroxybenzophenone (4,4'-DHBP) and 7-tridecanone.

Table 2

Inhibition of human 20S proteasome activity by RID-F derivatives and their cytotoxic effect on human cells (HEK293 and HL-60).

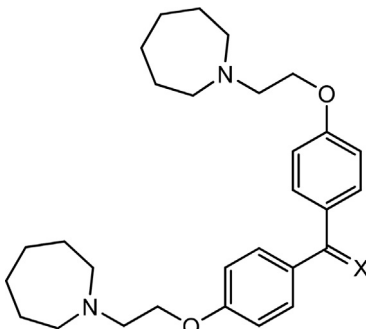
Compound number			IC ₅₀ (μM) ^a			HEK293	CyT ₅₀ (μM) ^b
			CT-L	T-L	PGPH		HL-60
							
9	RID-F-S*13	X = C(<i>c</i> -Hex)Ph	>10	>10	0.35 ± 0.02	>30	>30
10	RID-F-S*14	X = CPh ₂	1.18 ± 0.07	>10	0.37 ± 0.06	23.2 ± 1.1	>30
11	RID-F-S*12	X = C(<i>n</i> -C ₃ H ₇)Ph	1.37 ± 0.27	0.28 ± 0.04	1.05 ± 0.46	26.8 ± 1.0	4.30 ± 0.55
6	RID-F	X = C(C ₂ H ₅)Ph	0.64 ± 0.14	0.34 ± 0.12	0.43 ± 0.08	4.38 ± 0.79	3.42 ± 0.33
12	RID-F-S*11	X = C(CH ₃)Ph	0.90 ± 0.10	0.36 ± 0.17	0.87 ± 0.04	18.9 ± 1.2	6.87 ± 1.47
13	RID-F-S*1	X = CHPh	0.58 ± 0.05	0.69 ± 0.54	0.37 ± 0.19	6.06 ± 0.45	9.73 ± 0.62
14	RID-F-S*16	X = 	2.19 ± 0.25	2.18 ± 2.03	0.89 ± 0.09	12.5 ± 0.3	11.7 ± 0.4
15	RID-F-S*15	X = 	2.70 ± 0.10	1.11 ± 0.08	1.67 ± 0.15	26.2 ± 1.9	20.1 ± 0.6

^a IC_{50} values denote concentrations of the compounds required for 50% inhibition of the activities (see "Experimental section"). CT-L, chymotrypsin-like activity; T-L, trypsin-like activity; PGPH, peptidylglutamyl peptide hydrolase activity. NT, not tested.

^b CyT_{50} values denote concentration of the compounds required for 50% inhibition of the cell proliferation (see "Experimental section"). Values are means of triplicate.

Table 3Inhibition of 20S proteasome activity by RID-F derivatives substituted with aliphatic chains at the center sp^2 carbon (X) and their cytotoxic effect on human cells.

Compound number			IC_{50} (μM) ^a			HEK293	CyT_{50} (μM) ^b
			CT-L	T-L	PGPH		



16	RID-F-S*24	X = C(n -C ₆ H ₁₃) ₂	>10	>10	>10	>30	>30
17	RID-F-S*17	X = C(n -C ₅ H ₁₁) ₂	>10	>10	>10	14.5 ± 3.9	>30
18	RID-F-S*23	X = C(n -C ₄ H ₉) ₂	>10	>10	>10	>30	25.3 ± 0.6
19	RID-F-S*22	X = C(n -C ₃ H ₇) ₂	3.38 ± 0.42	>10	2.51 ± 0.44	>30	>30
20	RID-F-S*10	X = C(C ₂ H ₅) ₂	1.57 ± 0.70	0.96 ± 0.18	0.84 ± 0.12	6.02 ± 0.14	8.87 ± 1.13
21	RID-F-S*9	X = C(CH ₃) ₂	1.66 ± 0.12	>10	1.20 ± 0.19	11.1 ± 0.5	10.7 ± 1.6
22	RID-F-S*2	X = CH(C ₂ H ₅)	1.46 ± 0.14	1.61 ± 0.47	1.03 ± 0.10	26.7 ± 0.8	22.6 ± 0.3
23	RID-F-S*5	X = O	1.65 ± 0.21	8.59 ± 1.75	1.56 ± 0.08	13.9 ± 1.4	>30
24	RID-F-S*3	X = CH ₂	1.04 ± 0.22	0.88 ± 0.45	0.91 ± 0.04	9.80 ± 5.53	10.7 ± 0.5

^a IC_{50} values denote concentrations of the compounds required for 50% inhibition of the activities (see "Experimental section"). CT-L, chymotrypsin-like activity; T-L, trypsin-like activity; PGPH, peptidylglutamyl peptide hydrolase activity. NT, not tested.

^b CyT_{50} values denote concentration of the compounds required for 50% inhibition of the cell proliferation (see "Experimental section"). Values are means of triplicate.

whether the observed cytotoxicity of RID-F derivatives was due to apoptosis. MG132, a representative proteasome inhibitor that binds all three subunits, was used as a control compound. Cleavage of poly(ADP-ribose) polymerase (PARP) is one of the hallmarks of apoptosis. RID-F (**6**) (Fig. 5A) and RID-F-S*4 (**25**) (Fig. 5B) caused PARP cleavage in a dose-dependent manner, but PARP cleavage was almost undetectable in cells treated with RID-F-S*110 (**30**) (Fig. 5C), which was consistent with the very low inhibition of proteasome activities demonstrated by this compound (Table 5). RID-F-induced apoptosis was confirmed by cleavage of caspase 3 (Supplementary Fig. S1) and an increase in the proportion of cells in the sub-G1 fraction as determined by flow cytometry (Supplementary Fig. S2). These results indicate

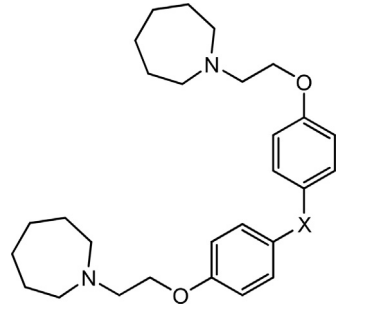
that the cytotoxicity of RID-F derivatives can be attributed at least in part to apoptosis.

2.6. Three-dimensional modeling of RID-F derivatives bound to the yeast proteasome subunit PRE3

How do RID-F derivatives bind the proteasome to exhibit their inhibitory effect? Docking studies were conducted to attempt to answer this question. To date, no reports of the experimental determination of the 3D structure of the human 20S proteasome have been published. However, several 3D structures of the yeast proteasome have been reported. The molecular structure of the ligand-binding pockets of the yeast and mammalian proteasomes is

Table 4Inhibition of 20S proteasome activity by RID-F derivatives with aliphatic side structures at the center sp^3 carbon (X) and their cytotoxic effect on human cells.

Compound number			IC_{50} (μM) ^a			HEK293	CyT_{50} (μM) ^b
			CT-L	T-L	PGPH		



25	RID-F-S*4	X = CH ₂	0.67 ± 0.04	0.99 ± 0.21	0.63 ± 0.15	10.9 ± 0.6	14.5 ± 0.3
26	RID-F-S*101	X = CH(CH ₃)	0.80 ± 0.02	>10	0.79 ± 0.02	8.12 ± 0.14	21.4 ± 0.6
27	RID-F-S*102	X = C(CH ₃) ₂	0.75 ± 0.01	1.87 ± 0.83	0.77 ± 0.01	7.61 ± 0.05	17.6 ± 1.8
28	RID-F-S*6	X = C(CH ₃)OH	1.66 ± 0.11	2.95 ± 0.40	1.35 ± 0.05	22.7 ± 6.3	7.06 ± 0.48
29	RID-F-S*103	X = C(CH ₂) ₂ CH ₂	1.94 ± 0.09	0.20 ± 0.20	1.08 ± 0.16	17.5 ± 0.3	>30

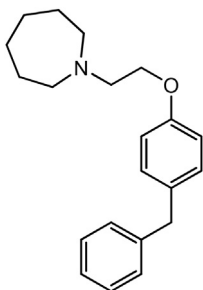
^a IC_{50} values denote concentrations of the compounds required for 50% inhibition of the activities (see "Experimental section"). CT-L, chymotrypsin-like activity; T-L, trypsin-like activity; PGPH, peptidylglutamyl peptide hydrolase activity. NT, not tested.

^b CyT_{50} values denote concentration of the compounds required for 50% inhibition of the cell proliferation (see "Experimental section"). Values are means of triplicate.

Table 5

Inhibition of 20S proteasome activity by a RID-F derivative missing one of the two homopiperidine rings and its cytotoxic effect on human cells.

Compound number		IC ₅₀ (μM) ^a			CyT ₅₀ (μM) ^b HEK293	HL-60
		CT-L	T-L	PGPH		
30	RID-F-S*110	>10	>10	>10	27.0 ± 3.7	>30



^a IC₅₀ values denote concentrations of the compounds required for 50% inhibition of the activities (see “Experimental section”). CT-L, chymotrypsin-like activity; T-L, trypsin-like activity; PGPH, peptidylglutamyl peptide hydrolase activity. NT, not tested.

^b CyT₅₀ values denote concentration of the compounds required for 50% inhibition of the cell proliferation (see “Experimental section”). Values are means of triplicate.

highly conserved [44,45]. Moreover, RID-F also inhibited yeast proteasome CT-L activity, with an IC₅₀ of 1.8 μM, which was similar to that (IC₅₀ 0.65 μM) determined for the human 20S proteasome (Table 1). These results suggest that the binding modes of the RID-F derivatives to the yeast and human proteasomes are similar. Therefore, we used the yeast proteasome structure for docking simulations of RID-F derivatives.

We used structure data of the yeast 20S proteasome complexed with fellutamide B (PDB ID: 3d29) for docking simulations. The PRE3 subunit (chain N) is the yeast counterpart of the human 20S proteasome β1 subunit, which exhibits PGPH activity. This subunit is sandwiched between the PUP1 subunit (chain H) and the PRE4 subunit (chain M) in the β ring, and the ligand-binding cleft of the PRE3 subunit is formed by these three subunits. Therefore, the trimer structure of chains H, N, and M was used for docking simulations. Using Molecular Operating Environment software, version 2010.10 (MOE 2010.10, Chemical Computing Group Inc.), the energy-minimized trimer structure with hydrogen atoms was prepared with the default parameters. The possible ligand-binding site in the trimer structure was detected using the Site Finder application of MOE 2010.10, with the Connection Distance parameter set to 1.9 Å. Docking simulations involving the RID-F derivatives and the trimer structure were then carried out using ASEDock [46], with the standard procedure.

The best-fitted inhibitor positions near in the active center Thr1 residue suggested that compounds **6** (RID-F), **9**, **10**, **11**, **12**, **13**, **14**, **15**,

20, **22**, and **23** (but not compounds **19**, **21**, **24** and **25** (RID-F-S*4)) have a similar binding mode. Fig. 6 (A and B) shows the highest-ranked binding mode of docked RID-F (**6**), illustrating molecular interactions between RID-F and the PRE3 catalytic site. One of the important points in the interaction between RID-F and the proteasome appears to be the contact area of the S1 pocket around Thr1. The vinyl benzene group in the side structure of RID-F is in contact with the S1 pocket and has a CH–π interaction with Thr21. The contacted residues delimit the binding pocket size at 120 Å³, in which Thr1 is located at the bottom. These docking simulation results are in agreement with the experimental evidence indicating that the size of the RID-F derivative side structure is critical for binding to the catalytic site.

As the exceptional case, docking simulations involving compounds **19**, **21**, **24**, and **25** (RID-F-S*4) showed one homopiperidine ring contacting the S1 pocket. Their side structures at the X position were either too large or too small. RID-F-S*4 (**25**), which has a high inhibition potency despite the absence of a side structure, binds in a different fashion, as shown in Fig. 6. One terminal homopiperidine moiety in RID-F-S*4 (**25**) enters into the binding cleft in the S1 pocket, as opposed to the vinyl benzene group of RID-F (**6**). These results imply that RID-F derivatives have two modes of binding to the catalytic sites. Interestingly, the results of the docking simulations involving compounds **19**, **21**, **24**, and **25** (RID-F-S*4) suggest that they access the active site in a manner different from that of compound **6** (RID-F), which contacts the active site via the vinyl

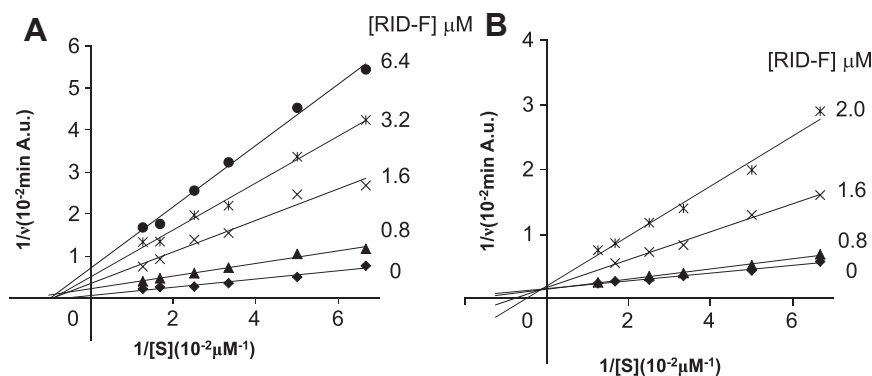


Fig. 1. Lineweaver–Burk plots of the inhibition of proteasomal CT-L and PGPH activities by RID-F. A, CT-L activity. B, PGPH activity. CT-L and PGPH activities were determined using a fluorometric assay as described in the Experimental section, varying the concentrations of substrate and RID-F as indicated. A.U. represents arbitrary units of fluorescence.

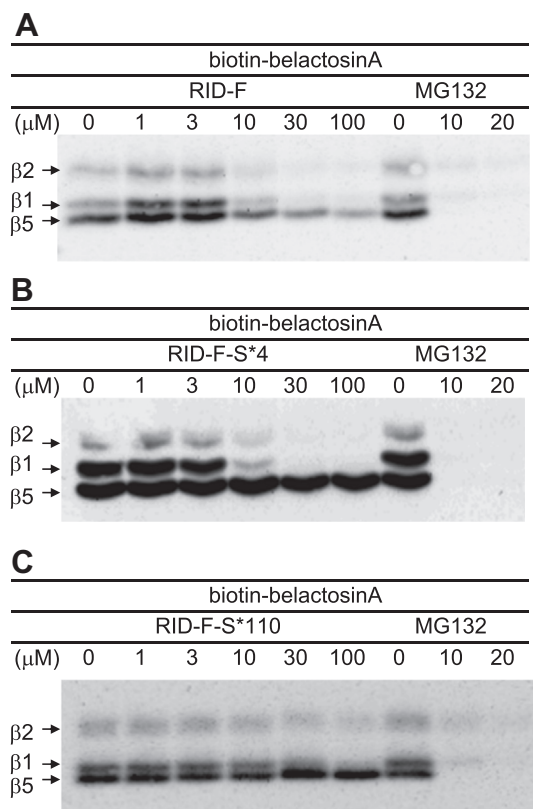


Fig. 2. Inhibition by RID-F derivatives of biotin-labeled belactosin A binding to the proteasome. As described in the [Experimental section](#), human 20S proteasomes were treated with biotin-belactosin A in the presence of RID-F (**6**) (A), RID-F-S*4 (**25**) (B), or RID-F-S*110 (**30**) (C), and biotin-labeled subunits (β1 for T-L activity, β2 for PGPH activity, and β5 for CT-L activity) were then detected. MG132 was used as a control.

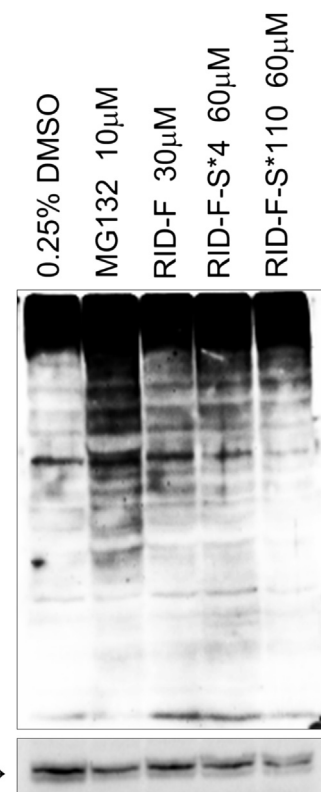


Fig. 4. Accumulation of ubiquitinated proteins induced by RID-F (**6**), RID-F-S*4 (**25**), and RID-F-S*110 (**30**). HeLa cells were treated with 0.25% DMSO (control), MG132 (10 μM), RID-F (30 μM), RID-F-S*4 (60 μM), or RID-F-S*110 (60 μM) for 24 h. Whole cell lysates were immunoblotted with anti-ubiquitin antibody. β-Actin was used as a loading control.

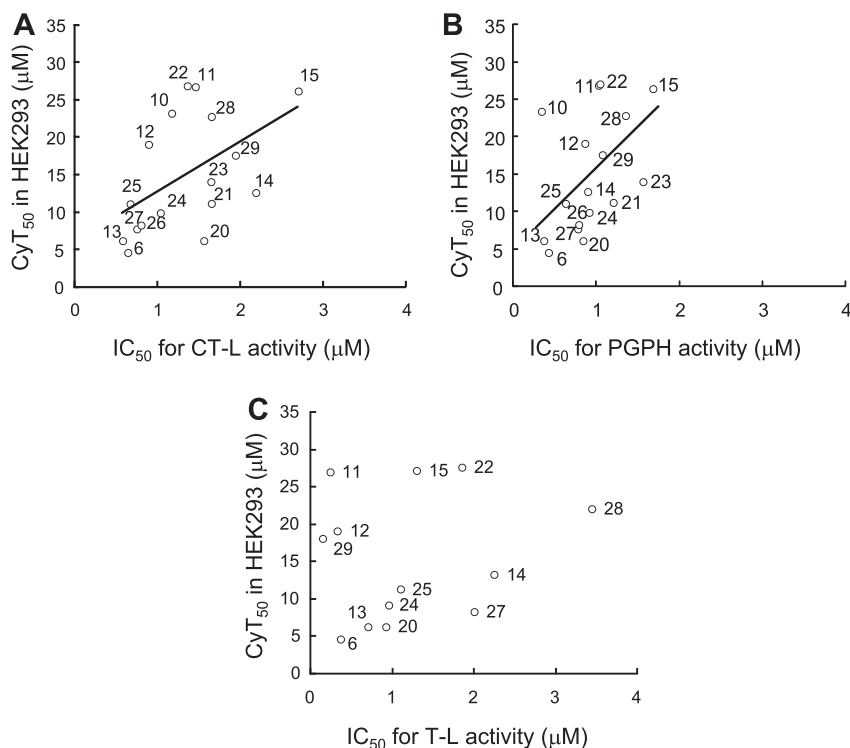


Fig. 3. Correlation between cytotoxicity (CyT₅₀) to HEK293 cells and inhibitory potency against the CT-L and PGPH activities of the human 20S proteasome. A, CyT₅₀ versus IC₅₀ for CT-L activity. B, CyT₅₀ versus IC₅₀ for PGPH activity. C, CyT₅₀ versus IC₅₀ for T-L activity. Numbers in the plots correspond to the compound numbers listed in [Tables 2–4](#).

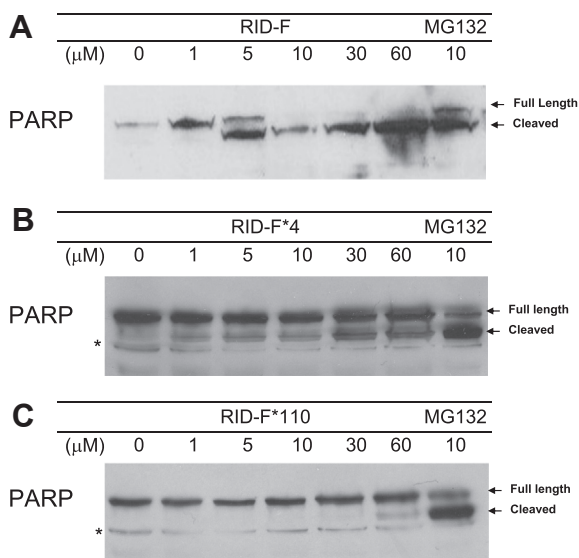


Fig. 5. Apoptosis induced by RID-F derivatives. HeLa cells were incubated with the compounds at indicated concentrations, after which cleavage of PARP was determined by Western blotting (see [Experimental section](#)). A, RID-F (**6**); B, RID-F-S*4 (**25**); C, RID-F-S*110 (**30**). MG132, a proteasome inhibitor that induces PARP cleavage, which is a hallmark of apoptosis, was used as a control. * = nonspecific bands.

benzene at the X position. As illustrated in [Fig. 6](#) (C and D) for RID-F-S*4 (**25**) as a representative, these RID-F derivatives may interact with the S1 pocket via one of the homopiperidine rings. The side structures at the X positions in these four compounds were too large or too small in comparison with the optimal size of vinyl benzene. Thus, it appears that not only the presence of two homopiperidine rings but also the relationship between the homopiperidine rings and the side structures at the X position are important for manifestation of the proteasome inhibition activity of the RID-F derivatives, suggesting that further studies of this relationship are warranted.

3. Conclusion

Ridaifen-F (RID-F), a novel tamoxifen derivative, inhibited the human 20S proteasome. The structure–activity relationship of a series of RID-F derivatives revealed the fundamental structures required for proteasome inhibition. The derivatives inhibited the proteasome in cells, inducing apoptotic cell death. Based on kinetic analyses of the inhibition and docking simulation, we propose the inhibition mode of RID-Fs. Our next trial is underway to develop highly potent RID derivatives for *in vivo* use.

4. Experimental section

4.1. 20S proteasome fluorometric substrate assay

CT-L, PGPH, and T-L proteasome activities were determined by measuring the degradation rates of the fluorometric substrates succinyl-LLVY-AMC, Z-LLE-AMC, and Boc-LRR-AMC, respectively. Purified human 20S proteasomes (0.1 μ g) were incubated with 50 μ M (CT-L) or 20 μ M (PGPH and T-L) fluorometric peptide substrate in the presence of varying concentrations of inhibitory compounds (0.01–10 μ M) in 100 μ L of assay buffer (25 mM HEPES, 0.5 mM EDTA, 0.03% SDS) at 37 $^{\circ}$ C. In the T-L activity assay, SDS was excluded from the assay buffer [47]. Reactions were monitored by AMC product formation (λ_{ex} = 380 nm, λ_{em} = 460 nm) for 1 h. The IC_{50} , defined as the compound concentration required for 50% inhibition of proteasome activity, was determined for each compound from the respective inhibition curve.

4.2. Growth inhibition assays

HEK293 cells (ER-negative) were cultured in Dulbecco's Modified Eagle Medium containing 10% fetal bovine serum, 100 units/mL of penicillin, and 0.1 mg/mL of streptomycin. HL-60 cells (ER-positive) were cultured in Iscove's Modified Dulbecco's Medium containing 10% fetal bovine serum, 100 units/mL of penicillin, and 0.1 mg/mL of streptomycin. Cells were seeded in duplicate wells in a 96-well plate

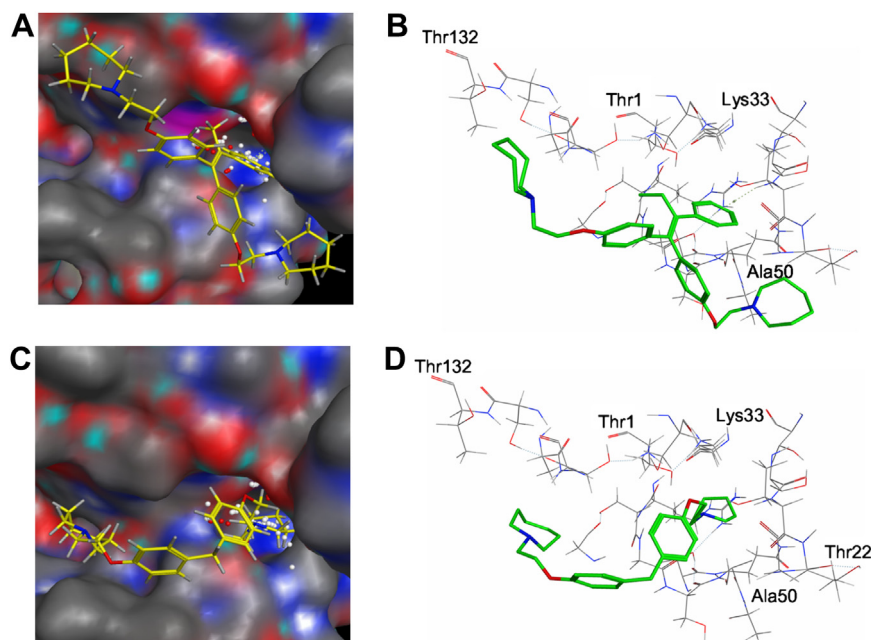


Fig. 6. Schematic view of RID-F (**6**) (panels A and B) or RID-F-S*4 (**25**) (panels C and D) – proteasome interactions. Images (panels A and C) represent the most likely binding modes. The binding pocket is shown as a solid surface with carbon atoms colored gray, N atoms colored blue, and O atoms colored red. Panels B and D show skeleton models of the binding modes.

at a density of 5×10^3 cells/well and were cultured for 48 h in medium alone or in medium containing an RID-F derivative at different concentrations (ranging from 0.1 to 20 μ M). Cell viability and proliferation were evaluated by quantification of MTT reduction by mitochondrial dehydrogenases. Formazan dye production was measured by determining the 560/750 nm absorbance ratio after HCl/2-propanol extraction according to the manufacturer's protocol (Promega). The CyT_{50} , defined as the compound concentration required for 50% inhibition of cell proliferation, was determined for each compound from the respective inhibition curve.

4.3. Binding experiment

Purified human 20S proteasomes were incubated with varying concentrations of RID-F derivatives or the representative proteasome activity inhibitor MG132 for 1 h at 37 °C and then biotin-belactosin A was added at 1 μ M. After an additional 1 h of incubation, proteins were separated by SDS-PAGE and transferred to a polyvinylidene difluoride (PVDF) membrane (Millipore). The membrane was blocked with 5% skim milk solution. Biotin-labeled proteins were visualized using streptavidin-HRP reagent and an ECL Plus membrane blot analysis detection kit (GE Healthcare).

4.4. Western blotting

HeLa cells (4×10^5 cells/well) were seeded in a 12-well plate and incubated with varying concentrations of RID-F derivatives for 24 h. The cells were then lysed with lysis buffer (62.5 mM Tris–HCl, 2% SDS, 10% glycerol, 0.1 mg/mL of phenylmethylsulfonyl fluoride, 10 μ g/mL of leupeptin, 1 μ g/mL of pepstatin A, and a phosphatase inhibitor cocktail (Nacalai Tesque Inc., Kyoto, Japan)). Equivalent amounts of protein (30 μ g) were resolved by SDS-PAGE, transferred and immobilized onto PVDF membranes, and probed with primary and secondary antibodies. Anti-ubiquitin antibody (1:200 dilution; Santa Cruz Biotechnology), anti-actin antibody (1:10,000; Santa Cruz Biotechnology), and HRP-conjugated anti-mouse or anti-rabbit antibody (1:2000; Santa Cruz Biotechnology) were used. Immunodetection was performed as described above.

Apoptosis induced by RID-F derivatives was examined with HeLa cells. Cells (4×10^5 cells/well) were seeded in a 12-well plate and incubated with varying concentrations of RID-F derivatives for 24 h. Cleavage of PARP, which is a hallmark of apoptosis, was detected by Western blotting as described previously [48].

Conflict of interest

The authors declare no competing financial interest.

Acknowledgment

The authors thank Mie Tsuchida and Miho Hosoi for technical assistance and Dr. Tetuo Yoshida of Kyowa Hakko Kirin Co. for supplying belactosin A. The authors also thank Drs. Takao Yamori and Reiko Shinkura for helpful discussions. This study was supported by a Health Labour Sciences Research Grant from the Ministry of Health, Labour and Welfare, Japan to I.S. and a Grant-in-Aid for Scientific Research on Priority Area "Cancer" from the Ministry of Education, Culture, Sports, Science and Technology, Japan to T.M. M.S. received support from the Platform for Drug Discovery, Informatics, and Structural Life Science of the Ministry of Education, Culture, Sports, Science and Technology, Japan.

Abbreviations

AMC 7-amino-4-methylcoumarin

CT-L	chymotrypsin-like
CyT_{50}	half-maximum cytotoxicity concentration
4,4'-DHBP	4,4'-dihydroxybenzophenone
DMF	dimethylformamide
ER	estrogen receptor
IC_{50}	half-maximum inhibitory concentration
HRP	horseradish peroxidase
K_i	inhibition constant
MTT	(3-(4,5-dimethylthiazol-2-yl)-2,5-diphenyltetrazolium bromide
PARP	poly-ADP ribose polymerase
PGPH	peptidylglutamyl peptide hydrolase
<i>p</i> -TsOH	<i>p</i> -toluenesulfonic acid
RID	ridaifen
SDS	sodium dodecyl sulfate
TAM	tamoxifen
T-L	trypsin-like
THF	tetrahydrofuran.

Appendix A. Supplementary data

Supplementary data related to this article can be found at <http://dx.doi.org/10.1016/j.ejmech.2013.11.009>.

References

- [1] A. Navon, A. Ciechanover, The 26S proteasome: from basic mechanisms to drug targeting, *J. Biol. Chem.* 284 (2009) 33713–33718.
- [2] A.G. Eldridge, T. O'Brien, Therapeutic strategies within the ubiquitin proteasome system, *Cell Death Differ.* 17 (2010) 4–13.
- [3] D. Hanahan, R.A. Weinberg, Hallmarks of cancer: the next generation, *Cell* 144 (2011) 646–674.
- [4] M.A. Shahshahan, M.N. Beckley, A.R. Jazirehi, Potential usage of proteasome inhibitor bortezomib (Velcade, PS-341) in the treatment of metastatic melanoma: basic and clinical aspects, *Am. J. Cancer Res.* 1 (2011) 913–924.
- [5] M.A. Gräwert, M. Groll, Exploiting nature's rich source of proteasome inhibitors as starting points in drug development, *Chem. Commun. (Camb.)* 48 (2012) 1364–1378.
- [6] P. Lawasut, D. Chauhan, J. Laubach, C. Hayes, C. Fabre, M. Maglio, C. Mitsiades, T. Hideshima, K.C. Anderson, P.G. Richardson, New proteasome inhibitors in myeloma, *Curr. Hematol. Malig. Rep.* 7 (2012) 258–266.
- [7] A. Mullard, Next-generation proteasome blockers promise safer cancer therapy, *Nat. Med.* 18 (2012) 7.
- [8] A. Katsnelson, Next-generation proteasome inhibitor approved in multiple myeloma, *Nat. Biotechnol.* (2012) 1011–1012.
- [9] A.A. Argyriou, G. Iconomou, H.P. Kalofonos, Bortezomib-induced peripheral neuropathy in multiple myeloma: a comprehensive review of the literature, *Blood* 112 (2008) 1593–1599.
- [10] L. Meng, R. Mohan, B.H. Kwok, M. Elofsson, N. Sin, C.M. Crews, Epoxomicin, a potent and selective proteasome inhibitor, exhibits in vivo anti-inflammatory activity, *Proc. Natl. Acad. Sci. U. S. A.* 96 (1999) 10403–10408.
- [11] J. Myung, K.B. Kim, K. Lindsten, N.P. Dantuma, C.M. Crews, Lack of proteasome active site allostery as revealed by subunit-specific inhibitors, *Mol. Cell* 7 (2001) 411–420.
- [12] D.J. Kuhn, Q. Chen, P.M. Voorhees, J.S. Strader, K.D. Shenk, C.M. Sun, S.D. Demo, M.K. Bennett, F.W. van Leeuwen, A.A. Chanan-Khan, R.Z. Orlowski, Potent activity of carfilzomib, a novel, irreversible inhibitor of the ubiquitin-proteasome pathway, against preclinical models of multiple myeloma, *Blood* 110 (2007) 3281–3290.
- [13] D. Chen, M. Frezza, S. Schmitt, J. Kanwar, Q.P. Dou, Bortezomib as the first proteasome inhibitor anticancer drug: current status and future perspectives, *Curr. Cancer Drug Targets* 11 (2011) 239–253.
- [14] E. Genin, M. Reboud-Ravaux, J. Vidal, Proteasome inhibitors: recent advances and new perspectives in medicinal chemistry, *Curr. Top. Med. Chem.* 10 (2010) 232–256.
- [15] G. Schmidtke, H.G. Holzthutter, M. Bogyo, N. Kairies, M. Groll, R. de Giuli, S. Emch, M. Groettrup, How an inhibitor of the HIV-1 protease modulates proteasome activity, *J. Biol. Chem.* 274 (1999) 35734–35740.
- [16] P. Furet, P. Imbach, P. Fuerst, M. Lang, M. Noorani, J. Zimmermann, C. Garcia-Echeverria, Structure-based optimisation of 2-aminobenzylstatine derivatives: potent and selective inhibitors of the chymotrypsin-like activity of the human 20S proteasome, *Bioorg. Med. Chem. Lett.* 12 (2002) 1331–1334.
- [17] P. Furet, P. Imbach, M. Noorani, J. Koeppeler, K. Laumen, M. Lang, V. Guagnano, P. Fuerst, J. Roesel, J. Zimmermann, C. Garcia-Echeverria, Entry into a new class of potent proteasome inhibitors having high antiproliferative activity by structure-based design, *J. Med. Chem.* 47 (2004) 4810–4813.

- [18] R.T. Lum, M.G. Nelson, A. Joly, A.G. Horsma, G. Lee, S.M. Meyer, M.M. Wick, S.R. Schow, Selective inhibition of the chymotrypsin-like activity of the 20S proteasome by 5-methoxy-1-indanone dipeptide benzamides, *Bioorg. Med. Chem. Lett.* 8 (1998) 209–214.
- [19] N. Basse, D. Papapostolou, M. Pagano, M. Reboud-Ravaux, E. Bernard, A.S. Felten, R. Vanderesse, Development of lipopeptides for inhibiting 20S proteasomes, *Bioorg. Med. Chem. Lett.* 16 (2006) 3277–3281.
- [20] C. Blackburn, K.M. Gigstad, P. Hales, K. Garcia, M. Jones, F.J. Bruzzese, C. Barrett, J.X. Liu, T.A. Soucy, D.S. Sappal, N. Bump, E.J. Olhava, P. Fleming, L.R. Dick, C. Tsu, M.D. Sintchak, J.L. Blank, Characterization of a new series of non-covalent proteasome inhibitors with exquisite potency and selectivity for the 20S $\beta 5$ -subunit, *Biochem. J.* 430 (2010) 461–476.
- [21] G. Lin, T. Chidawanyika, C. Tsu, T. Warrior, J. Vaubourgeix, C. Blackburn, K. Gigstad, M. Sintchak, L. Dick, C. Nathan, N.C-Capped dipeptides with selectivity for mycobacterial proteasome over human proteasomes: role of S3 and S1 binding pockets, *J. Am. Chem. Soc.* 135 (2013) 9968–9971.
- [22] Y. Koguchi, J. Kohno, M. Nishio, K. Takahashi, T. Okuda, T. Ohnuki, S. Komatsubara, TMC-95A, B, C, and D, novel proteasome inhibitors produced by *Apiospora montagnei* Sacc. TC 1093. Taxonomy, production, isolation, and biological activities, *J. Antibiot. (Tokyo)* 53 (2000) 105–109.
- [23] M. Groll, R. Huber, L. Moroder, The persisting challenge of selective and specific proteasome inhibition, *J. Pept. Sci.* 15 (2009) 58–66.
- [24] N. Basse, S. Piguel, D. Papapostolou, A. Ferrier-Berthelot, N. Richy, M. Pagano, P. Sarthou, J. Sobczak-Thépot, M. Reboud-Ravaux, J. Vidal, Linear TMC-95-based proteasome inhibitors, *J. Med. Chem.* 50 (2007) 2842–2850.
- [25] A. Desvergne, E. Genin, X. Maréchal, N. Gallastegui, L. Dufau, N. Richy, M. Groll, J. Vidal, M. Reboud-Ravaux, Dimerized linear mimics of a natural cyclopeptide (TMC-95A) are potent noncovalent inhibitors of the eukaryotic 20S proteasome, *J. Med. Chem.* 56 (2013) 3367–3378.
- [26] N. Basse, M. Montes, X. Marechal, L. Qin, M. Bouvier-Durand, E. Genin, J. Vidal, B.O. Villoutreix, M. Reboud-Ravaux, Novel organic proteasome inhibitors identified by virtual and *in vitro* screening, *J. Med. Chem.* 53 (2010) 509–513.
- [27] S. Mandlekar, A.N. Kong, Mechanisms of tamoxifen-induced apoptosis, *Apoptosis* 6 (2001) 469–477.
- [28] C. Ferlini, G. Scambia, M. Marone, M. Distefano, C. Gaggini, G. Ferrandina, A. Fattorossi, G. Isola, P. Benedetti Panici, S. Mancuso, Tamoxifen induces oxidative stress and apoptosis in oestrogen receptor-negative human cancer cell lines, *Br. J. Cancer* 79 (1999) 257–263.
- [29] Y. Kang, R. Cortina, R.R. Perry, Role of c-myc in tamoxifen-induced apoptosis estrogen-independent breast cancer cells, *J. Natl. Cancer Inst.* 88 (1996) 279–284.
- [30] Y. Nagahara, I. Shiina, K. Nakata, A. Sasaki, T. Miyamoto, M. Ikekita, Induction of mitochondria-involved apoptosis in estrogen receptor-negative cells by a novel tamoxifen derivative, ridaifen-B, *Cancer Sci.* 99 (2008) 608–614.
- [31] I. Shiina, Y. Sano, K. Nakata, T. Kikuchi, A. Sasaki, M. Ikekita, Y. Nagahara, Y. Hasome, T. Yamori, K. Yamazaki, Synthesis and pharmacological evaluation of the novel pseudo-symmetrical tamoxifen derivatives as anti-tumor agents, *Biochem. Pharmacol.* 75 (2008) 1014–1026.
- [32] I. Shiina, Y. Sano, K. Nakata, M. Suzuki, T. Yokoyama, A. Sasaki, T. Orikasa, T. Miyamoto, M. Ikekita, Y. Nagahara, Y. Hasome, An expeditious synthesis of tamoxifen, a representative SERM (selective estrogen receptor modulator), via the three-component coupling reaction among aromatic aldehyde, cinnamyltrimethylsilane, and β -chlorophenetole, *Bioorg. Med. Chem.* 15 (2007) 7599–7617.
- [33] I. Shiina, Y. Sano, K. Nakata, T. Kikuchi, A. Sasaki, M. Ikekita, Y. Hasome, Synthesis of the new pseudo-symmetrical tamoxifen derivatives and their anti-tumor activity, *Bioorg. Med. Chem. Lett.* 17 (2007) 2421–2424.
- [34] I. Shiina, M. Ikekita, T. Matsunaga, Y. Nagahara, Anticancer agent containing tamoxifen analogue as active ingredient, *Jpn. Kokai Tokkyo Koho* (11 May 2006). JP2006117648.
- [35] I. Shiina, Proteasome inhibitor which contains tamoxifen analogue as an active ingredient, *Jpn. Kokai Tokkyo Koho* (24 April 2008). JP2008094836.
- [36] T. Mukaiyama, Titanium tetrachloride in organic synthesis, *Angew. Chem. Int. Ed.* 16 (1977) 817–826.
- [37] D.D. Yu, B.M. Forman, Simple and efficient production of (Z)-4-hydroxytamoxifen, a potent estrogen receptor modulator, *J. Org. Chem.* 68 (2003) 9489–9491.
- [38] M.L. Connolly, The molecular surface package, *J. Mol. Graphics* 11 (1993) 139–141.
- [39] M. Hendlich, F. Rippmann, G. Barnickel, LIGSITE: automatic and efficient detection of potential small molecule-binding sites in proteins, *J. Mol. Graph. Model.* 15 (1997) 359–363.
- [40] T.D. Penning, N.S. Chandrakumar, B.B. Chen, H.Y. Chen, B.N. Desai, S.W. Djuric, S.H. Docter, A.F. Gasielki, R.A. Haack, J.M. Miyashiro, M.A. Russell, S.S. Yu, D.G. Corley, R.C. Durley, B.F. Kilpatrick, B.L. Parnas, L.J. Askonas, J.K. Gierse, E.I. Harding, M.K. Highkin, J.F. Kachur, S.H. Kim, G.G. Krivi, D. Villani-Price, E.Y. Pyla, W.G. Smith, N.S. Ghoreishi-Haack, Structure–activity relationship studies on 1-[2-(4-phenylphenoxy)ethyl]pyrrolidine (SC-22716), a potent inhibitor of leukotriene A₄ (LTA₄) hydrolase, *J. Med. Chem.* 43 (2000) 721–735.
- [41] M. Hasegawa, K. Kinoshita, C. Nishimura, U. Matsumura, M. Shionyu, S. Ikeda, T. Mizukami, Affinity labeling of the proteasome by a belactosin A derived inhibitor, *Bioorg. Med. Chem. Lett.* 18 (2008) 5668–5671.
- [42] W. Heinemeyer, J.A. Kleinschmidt, J. Saidowsky, C. Escher, D.H. Wolf, Proteinase yscE, the yeast proteasome/multicatalytic-multifunctional proteinase: mutants unravel its function in stress induced proteolysis and uncover its necessity for cell survival, *EMBO J.* 10 (1991) 555–562.
- [43] R. Gueckel, C. Enenkel, D.H. Wolf, W. Hilt, Mutations in the yeast proteasome beta-type subunit Pre3 uncover position-dependent effects on proteasomal peptidase activity and *in vivo* function, *J. Biol. Chem.* 273 (1998) 19443–19452.
- [44] M. Groll, L. Ditzel, J. Löwe, D. Stock, M. Bochtler, H.D. Bartunik, R. Huber, Structure of 20S proteasome from yeast at 2.4 Å resolution, *Nature* 386 (1997) 463–471.
- [45] M. Unno, T. Mizushima, Y. Morimoto, Y. Tomisugi, K. Tanaka, N. Yasuoka, T. Tsukihara, The structure of the mammalian 20S proteasome at 2.75 Å resolution, *Structure* 10 (2002) 609–618.
- [46] J. Goto, R. Kataoka, H. Muta, N. Hirayama, ASEDock-docking based on alpha spheres and excluded volumes, *J. Chem. Inf. Model.* 48 (2008) 583–590.
- [47] K. Tanaka, T. Yoshimura, A. Ichihara, Role of substrate in reversible activation of proteasomes (multi-protease complexes) by sodium dodecyl sulfate, *J. Biochem. (Tokyo)* 106 (1989) 495–500.
- [48] T. Kunoh, T. Noda, K. Koseki, M. Sekigawa, M. Takagi, K. Shin-ya, N. Goshima, S. Iemura, T. Natsume, S. Wada, Y. Mukai, S. Ohta, R. Sasaki, T. Mizukami, A novel human dynactin-associated protein, dynAP, promotes activation of Akt, and ergosterol-related compounds induce dynAP-dependent apoptosis of human cancer cells, *Mol. Cancer Ther.* 9 (2010) 2934–2942.